Microchim Acta
DOI 10.1007/s00604-015-1698-y

ORIGINAL PAPER

SERS based point-of-care detection of food-borne pathogens

Nawfal Adam Mungroo[1] · **Gustavo Oliveira**[1] · **Suresh Neethirajan**[1]

Received: 20 September 2015 / Accepted: 1 December 2015
© Springer-Verlag Wien 2015

Abstract The authors have developed a microfluidic platform for improved detection of pathogenic bacteria by using silver nanoparticles and new platforms for chemometric data analysis, viz. a combination of principle component analysis and linear discriminant analysis. The method can distinguish eight key foodborne pathogens (*E. coli*, *S. typhimirium*, *S. enteritis*, *Pseudomonas aeruginosa*, *L. monocytogenes*, *L. innocua*, *MRSA 35* and *MRSA 86*) and, hence, holds good promise for use in the food industry.

Keywords Microfluidics · Food safety · Food analysis · Principle component analysis · Linear discriminant analysis · Silver nanoparticles · Raman spectroscopy

Introduction

Foodborne illnesses are responsible for about 20 million deaths annually worldwide [1]. In the United States alone, there have been a reported 48 million cases of foodborne illness with 128,000 hospitalizations and 3000 deaths annually [2]. Common foodborne bacteria include *Salmonella* species and *Escherichia coli 0157:H7* [3], among others.

Salmonella is a Gram-negative bacterium with over 2463 serotypes (serovars); the most common foodborne strains are *Salmonella typhimurium* and *Salmonella enteritidis* [4]. Salmonella infection is characterized by acute fever, diarrhea, gastroenteritis, and vomiting. Gastroenteritis is primarily caused by the *Typhimurium* serotype; globally there have been 1.3 billion cases of *Typhimurium* gastroenteritis and 3 million reported annual deaths. The mortality rate in developed countries is approximately 1 % compared to 24 % in developing countries. *Salmonella enterica* infections lead to typhoid fever, which is less common. There are approximately 17 million cases of typhoid fever and 500,000 annual deaths [5, 6]. *E. coli* is a Gram-negative bacterium also found in the gut of humans and warm-blooded animals. Some strains/serotypes of *E. coli* do not cause serious foodborne illness, although *E. coli O157:H7* is particularly problematic. Approximately 10 % of *E. coli* infected patients progress towards hemolytic uremic syndrome (HUS) with a mortality rate of 3 to 5 % [7].

Many other organisms can cause significant foodborne illnesses. *P. aeruginosa* is a Gram-negative bacterium that is highly resistant to most antibiotics. In the USA, *P. aeruginosa* infection accounts for 51,000 reported foodborne infections annually, 6000 (13 %) of which were multidrug-resistant. *P. aeruginosa* foodborne illness results in roughly 400 deaths per year in the US alone [8–10]. *L. monocytogenes* and *L. innocua* are Gram-positive psychrotrophic bacteria. *Listeria*-related casualties are common in the food industry due to ready transmission to humans from food products. The fatality rate for *Listeria* infection is relatively high, ranging from 20 to 30 %. With an increase in *Listeria* outbreaks occurring during the last few decades, governments are reinforcing their food safety policies to reduce the incidence of *Listeria* infection [10]. *MRSA* is another troublesome Gram-positive bacterium that is resistant to antibiotics. Consuming *MRSA*-contaminated foods can result in severe toxin-mediated illness including, diarrhea, vomiting, nausea, gastroenteritis, and abdominal pain within 1–6 h of ingestion. In recent years, there has been an increase in *MRSA*-related pathologies. For example, about 0.8 % of the US

✉ Suresh Neethirajan
sneethir@uoguelph.ca

[1] Bionano Laboratory, School of Engineering, University of Guelph, Guelph, ON N1G 2W1, Canada

Published online: 15 December 2015

population is affected by *MRSA*, and there was a 17-fold increase of *MRSA* infection reported in Canada from 1995 to 2000 [11, 12].

Aside from health concerns, foodborne illnesses are responsible for economic losses worth billions of dollars worldwide. For instance, the direct costs associated with foodborne illnesses include diagnosis, treatment, and management of the illness. Indirect costs include operational expenditures for healthcare facilities and personal transportation [13]. As evidence, foodborne illnesses in the US account for $10–83 billion spent annually [14].

To reduce the likelihood of foodborne illnesses, early and effective detection of pathogens is essential. Conventional practices commonly involve cultivating sample cells in laboratory settings, making it time-consuming and costly [15]. The most common techniques used for the detection of bacteria in food processing are enzyme-linked immunosorbent assays (ELISAs) and polymerase chain reaction (PCR) assays. ELISA based techniques are highly sensitive with detection limits as low as tens of picograms of protein per milliliter of sample [16]. However, there is a consensus among researchers that this recognition technique is not practical for onsite detection of bacteria. This is because ELISA is complex multi-step assay that is time-consuming, costly, and labor intensive [17]. PCR is a molecular technique used for in vitro amplification of DNA fragments using enzymatic replication [18]. Advantages include detection rates as low as 10–100 cells per milliliter of sample. However, PCR is also time and labor intensive, can take several hours (5 to 24 h), and requires skilled/trained personnel to perform and analyze the test. Additionally, this technique cannot distinguish between live and dead organisms, potentially detecting organisms that are not viable/hazardous [19]. Therefore, biosensors have been recognized as more effective alternatives to these techniques.

Surface Enhanced Raman Spectroscopy (SERS) is a label-free biosensing technique recently used for bacterial detection. When subjected to analytes (bacteria), Raman signals provide information about their chemical structures. Under ideal conditions, SERS is able to detect a single molecule using the intrinsic vibrational fingerprint of the detected analytes [20]. Additionally, Raman spectroscopy performance is not affected by the surrounding water, making this system adequate for bacteria detection [21, 22].

A combination of microfluidics, chemometric analysis and Raman spectroscopy provides a sustainable method to detect and confirm the presence of bacteria. Here we use principle component analysis (PCA), a statistical tool that reduces dimensionality of complex multivariate data while maintaining maximum variance, and linear discriminant analysis (LDA), a classification technique that uses the information in a learning set of labeled observations to construct a classifier (or classification rule) that will separate the predefined classes as much as possible.

To address the growing concern of food safety, a microfluidic based biosensing system integrating procedures involving a combination of Raman spectroscopy and chemometric analysis was developed. This procedure uses silver nanoparticles (AgNP) and Triton x-100 to discriminate between eight different foodborne pathogens (*E. coli*, *S. typhimirium*, *S. enteritis*, *P. aeruginosa*, *L. monocytogenes*, *L. innocua*, *MRSA* 35 and *MRSA* 86).

Experimentals

Materials

Bacterial cell suspensions of *E. coli*, (ATCC 25992) *S. tymphirium*, *S. enteritis*, *P. aeruginosa* BK-76, *L. monocytogenes* 1892, *L. innocua*, *MRSA* 35, and *MRSA* 86 (gifts from the Canadian Research Institute for Food Safety (CRIFS) and the Ontario Veterinary College Hospital of the University of Guelph) were grown overnight at 37 °C and 150 rpm in tryptone soy broth (TSB; Oxoid Canada, Nepean, ON). The bacterial cultures were then washed twice in water by centrifugation at 4500 g for 10 min at 4 °C, resuspended in water, and maintained at 4 °C until further analysis.

For treatment, cells were centrifuged at 4500 g for 10 min at 4 °C, which was quickly followed by resuspension in 200 μL of $NaBH_4$ solution (0.5 M). The mixture was then centrifuged at 4500 g for 10 min at 4 °C followed by addition of 200 μL of 0.1 % Triton x-100 (*v*/*v*) and incubation for 5 min. The next step involved adding 10 μL of $NaBH_4$ (0.5 M) with 800 μL of $AgNO_3$ (1 M) (Sigma Aldrich). To ensure optimum uniformity of samples, each sample was vortexed for 30 s, followed by 30 s of sonification, prior to analysis under the benchtop Raman spectrometer (Sierra Snowy Range 785 series, Laramie, WY). For the polymicrobial mixtures, 50 μL of bacterial suspensions were mixed followed by vortexing for 1 min. Prior to the measurement, each sample was vortexed for 30 s, followed by 30 s of sonification, before analysis under the benchtop Raman spectrometer.

Synthesis of silver nanoparticle (AgNP)

Seventy-five mL of milliQ water were added to a round bottom flask with 20 mL of 1 % (*w*/*v*) trisodium citrate dihydrate ($C_6H_9Na_3O_9$), which was heated to 70 °C for 15 min. A total of 1.7 mL of 1 % (*w*/*v*) $AgNO_3$ was added to the mixture, followed by the quick addition of 2 mL of 0.1 % (*w*/*v*) $NaBH_4$ solution. The reaction solution was kept under stirring at 70 °C. The mixture was then cooled to room temperature, and water was added to bring the volume to 100 mL. The resulting AgNPs were used as starter seeds.

Seventy-five mL of water was mixed with 2 mL of 1 % citrate solution and brought to boiling for 15 min. Afterward, 10 mL of starter seed solution and 1.7 mL of 1 % $AgNO_3$ solution were added and kept under stirring for 1 h. Lastly, 2 mL of 1 % citrate solution and 1.7 mL of 1 % $AgNO_3$ solution were added and kept in continuous stirring for another hour. This step was repeated every hour for 2 h. Finally, the reaction solution was cooled to room temperature. Water was added to bring the volume to 100 mL. The reaction solution was centrifuged at 5000 g for 10 min at 4 °C and washed twice in milliQ water. AgNPs were resuspended in milliQ water, sonicated for 15 min, and stocked at room temperature.

Design and fabrication of microfluidic chip

The microfluidic chip consisted of two inlets and one outlet connected with a capillary pump. The bacterial inlets (Fig. 1) and the associated AgNPs inlets were used to load the bacterial sample matrix solutions and the silver nanoparticle-triton mixture solution. Solutions were sequentially dispensed by hand using a syringe. The fabrication of the microfluidic chip followed standard photolithography and soft lithography. Briefly, it involved making a silicon wafer master mold and Polydimethylsiloxane (PDMS) chips. The master mold bearing the desired microchannel layout was made by depositing a layer of 80 μm UV cured SU-8 2025 negative photoresist (MicroCHEM, USA) onto the surface of the wafer. A PDMS chip was made with a soft lithography technique by using the master mold. A degassed mixture of PDMS prepolymer and curing agent (10:1 *w*/*w*, Sylgard, Dow Corning, Burlington, ON, Canada) was poured onto the mold and cured for 4 h at 75 °C. Solidified PDMS replica was then peeled off of the master mold, punched to form the inlets and outlet, and bonded onto a glass slide (25 × 75 × 1 mm, VWR International, Suwanee, GA, USA) after oxygen plasma treatment for 40 s. A position marker was used to facilitate the alignment between the sensing well and the sensing window when conducting the bonding.

Data collection

Ten μL of each bacterial suspension was pippetted onto the Q-SERS substrate (Nanova Inc., Columbia, MO, USA). A total of 5 replicates of each bacterial species were measured. Spectra were recorded using a benchtop Raman spectrometer (Sierra Snowy Range 785 series, Laramie, WY) under an excitation wavelength of 785 nm. The exposure time was 1 s, and the number of accumulations for each measurement was 10. The spectral data were acquired over a Stokes Raman shift of 400–2000 cm^{-1}. To diminish uniformity issues, each spectrum were collected in the raster mode. To ensure the satisfactory shape and size of AgNPs, the following tests were performed. Transmission Electron Microscopy (TEM) images

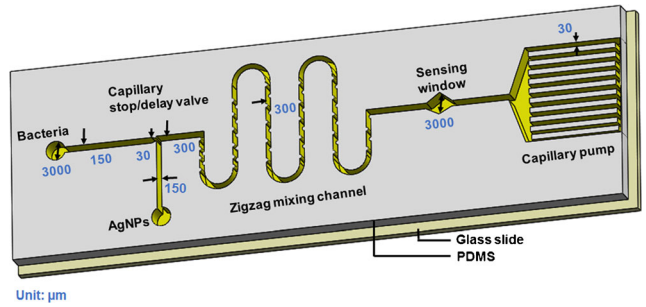

Fig. 1 Schematic of the integrated lab-on-a-chip for SERS based point-of-care biosensing system. SERS substrate was bonded under the sensing window for RAMAN spectral acquisition of the bacterial samples

were acquired using the FEI Tecnai G2 F20 instrument. These images will provide information about the shape and arrangement of the AgNPs. The UV visible spectrum was obtained using the Agilent Cary 300 UV-Vis in aqueous medium. The Dynamic Light Scattering (DLS) data which provides information about the size distribution was acquired using the Brookhaven NanoBrook Omni Particle Size Analyzer.

Data analysis

The SERS spectral data was analyzed using principal component analysis (PCA) and linear discriminant analysis (LDA) using IBM SPSS (V. 22). Spectral data were pre-processed by means of baseline correction, mean centering, and normalization using OriginPro software. Before multivariate analysis, each spectral feature was standardized. PCA was performed to identify spectral features specific to each bacterial type. LDA was performed to evaluate whether the treatment would improve the discrimination of different bacterial groups.

Results and discussion

The typical behavior of local EM enhancement is modeled as follows. Initially, EM increases with increasing AgNP sizes, yet beyond a threshold/optimum size these particles absorb less light intensity and scatter more through inelastic scattering, which causes a decrease in the overall SERS intensity. An increase in the size of the AgNP at a fixed concentration of Ag results in a decrease in the total surface area for adsorption, which can offset the EM field. Additionally, the attachment of AgNP to the bacteria plays an important role in the performance of the Raman output. For instance, direct attachment of synthesized AgNPs on the surface of bacteria provides a highly sensitive, effective (2× enhancement for 785 nm laser) and quick approach to detect bacteria on a microarray platform. In order to obtain optimum results, adequate attachment technique must be used alongside improved Surface Plasmon Resonance absorption of AgNP. Optimizing AgNP is

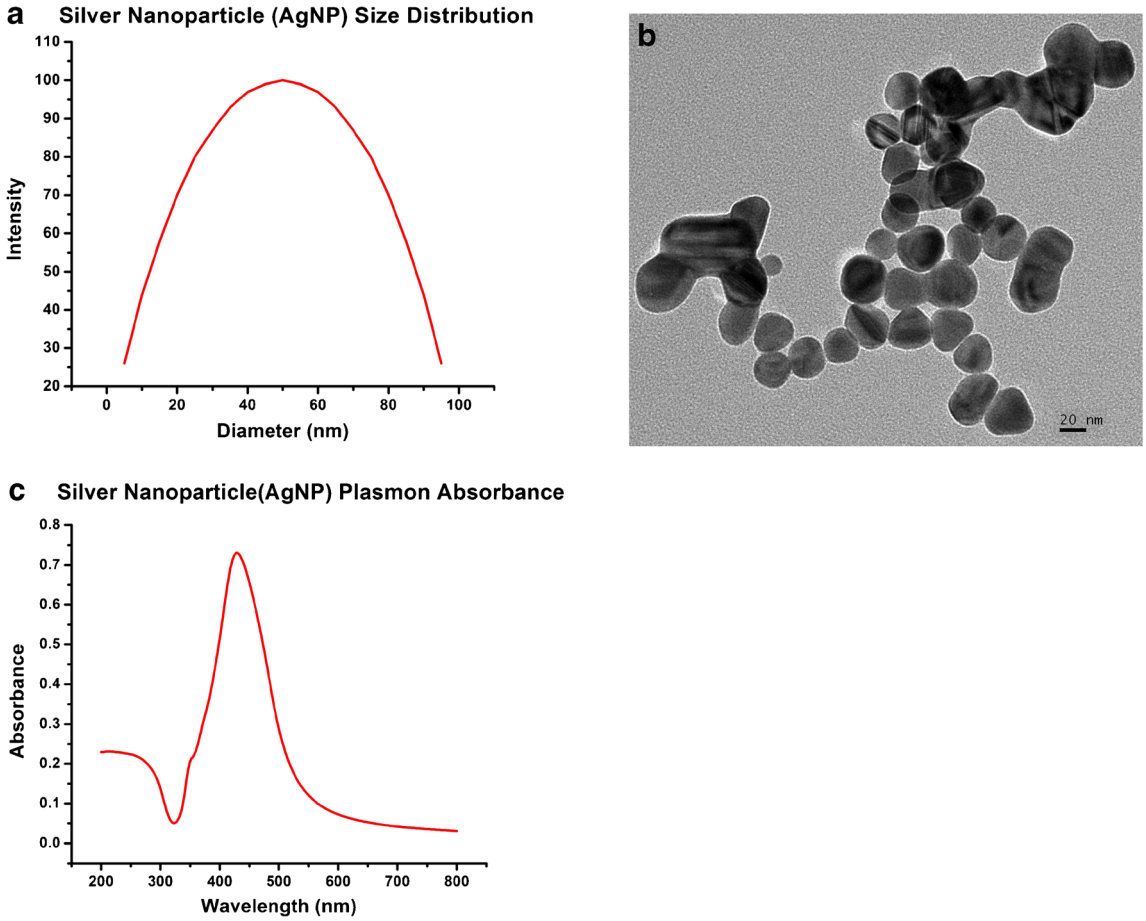

Fig. 2 **a** AgNP size distribution. **b** TEM images showing the size and shape of AgNP. **c** UV-visible spectrum of silver nanoparticles (AgNp) in aqueous medium

dependent on several elements, such as the shape and size of the particles, the inter-particle distance, and the dielectric constants, for which both the metal and the surface must be of satisfactory condition (no scratches or damage). Sodium borohydride was used as the ligand. Silver nanoparticles synthesized in the presence of $NaBH_4$ were reduced and stabilized with homogeneous particle size distribution between 10 to 90 nm. In the case of spherical AgNP, the Plasmon absorption is centered at ~400 nm, while the exact peak position is dependent on the size of the particles [23].

As observed in the transmission electron microscopic (TEM) images in Fig. 2b, the AgNP are spherical or quasi-

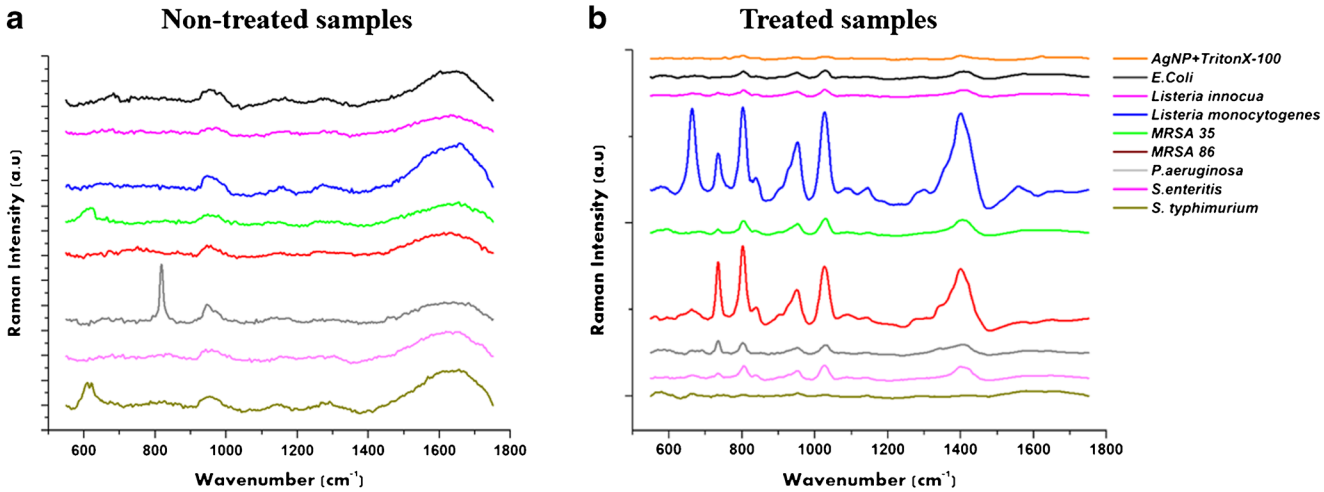

Fig. 3 **a** Averaged Raman spectrum of untreated bacterial samples, and **b** bacterial samples treated with AgNPs & Triton

spherical in shape, are closely packed together, and are fairly homogenous in size. The size distribution of the AgNP has been estimated to be 40 nm in diameter using dynamic light scattering techniques, as illustrated in Fig. 2a and c also shows the maximum plasmon absorbance is 435 nm, confirming the spherical or nearly-spherical nature of the AgNP.

As observed in Fig. 3b, there is an enhanced signal in the Raman peaks of the treated samples compared to the untreated samples. The treatment with AgNP and Triton resulted in suppression, creation, and the enhancement of Raman peaks. It is to be noted that assigning peaks visually is not an ideal practice, as there are generally a number of significant peaks that are not apparent/visible from the Raman spectrum displayed in Fig. 3b. To be able to distinguish the important peaks, PCA loading plot (Fig. 4c) distinguishes the important peaks from the obtained RAMAN spectra. The loading plot contains information about the different wavelengths that form the basis for unique fingerprinting of each bacterial species. The peaks obtained are compared to the literature to confirm and establish the effectiveness of our methodology. As observed in Table 1 this procedure performed relatively well and is largely in agreement with the peaks observed by other researchers from the literature. Results for *L. monocytogenes* and *MRSA 86* are better correlated with other studies, compared to the other bacterial strains tested.

Following preprocessing of the data, chemometric analysis is performed. Figure 4a and b illustrate the PCA output for the averaged bacterial sample. PCA factors 1 and 2 represent 68.4 % of the total variance present for the non-treated samples and 88.5 % for treated samples. The treated bacterial

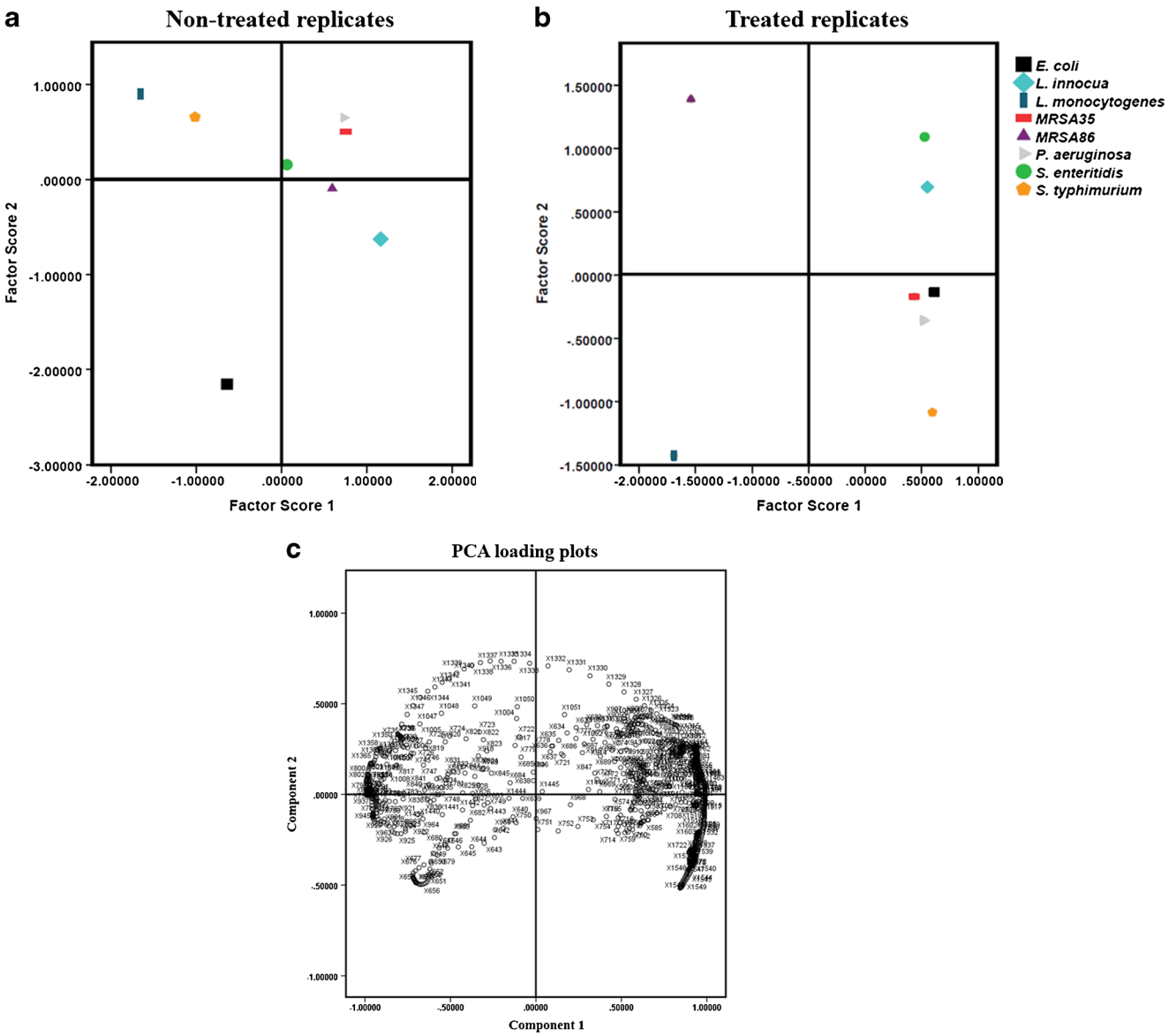

Fig. 4 PCA output for **a** untreated bacterial samples. **b** treated bacterial samples. **c** PCA loading plots showing specific macromolecular assigned Raman shift wavenumbers

Table 1 Peak positions and tentative assignment of the Raman spectral peaks identified in Figs. 2 and 5 for 8 food-borne bacterial pathogens used in the study based on the recent literature [11, 21, 25, 26, 27]

Raman shift (cm^{-1}) (Literature)	Raman shift (cm^{-1}) (This study)	Macromolecular assignment
MRSA 86		
546	550, 585	Carbohydrate
659, 672	647	δ deformation (guanine), ν (C-S) in cysteine.
749	743	Tryptophan
835	820	ν stretching (C-C) in 1,4 glycosidic link
894	888	Phosphodiester backbone, deoxyribose
946	957	Phospholipids N-C stretching
1043	1042, 1079	CC ring breathing (polysaccharide)
1134	1133	ν stretching (COC), ring breathing
1273	1250	Amide I
1408	1400	ν stretching (CO) symmetric COO-
1511	1535	Phenylalanine
1650	1650	Amide I, protein
MRSA 35		
556	550	Carbohydrate
692	647	(C-C) twist aromatic ring in tyrosine
748	752	Tryptophan
835	839	ν (C-C) in 1,4 glycosidic link
942	930	Phospholipids N-C stretching
1043	1020, 1065	CC ring breathing (polysaccharide)
1132	1120	ν stretching (COC), ring breathing
1410	1400	ν stretching (CO) symmetric COO-
S. *enteritis*		
620,690	590 633	C–C twist aromatic ring structure in tyrosine amino acid chain and guanine ring region of DNA/RNA, respectively.
858	812, 839	C–C stretch in 1,4 glycosidic link. These bands are due to the presence of carbohydrates, amino acid side chains, and lipids in bacteria cell wall.
930	957	Membrane phospholipids.
1050	1042	Probably due to the stretching model of C–O bond in $–CH_2OH$ of cell wall lipids.
1450	1425	Characteristic to C–H deformation bond of cell wall carbohydrate.
S. *typhimurium*		
570	550–580	Cell wall and cell membrane
658, 661	659	C–S stretch model of cysteine amino acid or Guanine present in protein
831	820	O-P-O stretching or tyrosine
930	950	Membrane phospholipids
1 173	1152	15-Methylpalmitic acid or acetoacetate
1 530	1550	Adenine, cytosine, guanine
E. coli		
858	820	Ribose, ν (COC)
928–937 928	930	C–COO− stretch (carbohydrates)
1 027	1011	A ring stretching, or (C-H) deformation
1 368	1358	Not specified
1450–1453 1450	1452	C–H deformation (lipids)
1,583 ~ 1,604 1,583	1570	Tyrosine (proteins)

Table 1 (continued)

Raman shift (cm^{-1}) (Literature)	Raman shift (cm^{-1}) (This study)	Macromolecular assignment
L. *monocytogenes*		
517, 543–550 543	550	S–S stretch (proteins)
713–734	752	Adenine (nucleic acids)
860	820, 839	Ribose, ν stretching (COC)
893	888	Phosphodiester backbone, deoxyribose
960	957	Phospholipids N-C stretching
1,003	1004	Phenylalanine (the symmetric ring breathing mode) (proteins)
1043	1042	CC ring breathing (polysaccharide)
1130	1132	ν stretching (COC), ring breathing
1275	1250	Amide I
1322, 1329, 1325, 1335	1358	Adenine (nucleic acids), associated with CH_3CH_2 vibrational modes
1,568–1,590 ~ 1,604	1560	Tyrosine (proteins)
1653, 1667	1650	Amide I, protein
L. *innocua*		
724	722	Deformational vibration of adenine
780	776	Cytosine or uracil (nucleic acids)
960	975	Phospholipids N-C stretching
P. *aeruginosa*		
546	550	Carbohydrate
659, 674	659, 693	δ deformation (guanine), ν (C-S) in cysteine
757	752	Tryptophan
797	790	Cytosine
857	839	Ribose, ν stretching (COC)
962	957	Phospholipids N-C stretching
1040	1011	CC ring breathing (polysaccharide)
1411	1415	ν stretching (CO) symmetric COO-
1403	1400	*ν* stretching (CO) symmetric COO-

spectral data tend to be more spread out, indicating improved discrimination. However, the spectral data of *MRSA 35* and *P. aeruginosa* are close to each other when untreated, translating to poor discrimination between these species.

The LDA output shows that only 27.5 % of the groups are correctly cross-validated for the non-treated as opposed to 97.5 % for the treated samples. This clearly indicates that the treatment provides superior discrimination of these bacterial species. These observations are visually represented in the LDA plots of each replicate. The treatment replicates are closely packed, and each spectral data from individual species is spread out (Fig. 5). The replicates from the non-treated cultures are not closely packed and each species is scattered, indicating unsatisfactory discrimination. In conclusion, both forms of chemometric analysis confirm better discrimination with treatment as opposed to the pure (untreated) cultures.

Once these protocols are validated, the next step is to further test their ability to distinguish species within polymicrobial cultures to simulate a more realistic industry scenario. The polymicrobial cultures are prepared in a 1:1 ratio for all samples. The mixtures are divided into three different categories. The mixtures were divided into three categories. The first was used to test whether the protocols can differentiate between species (e.g. between Salmonella and Listeria). The second category involves testing whether this method was able to discriminate Gram-positive and Gram-negative bacteria. The last category entailed mixing all eight bacterial samples together in the 1:1 ratio for comparisons (Fig. 6).

As observed in Fig. 7, factors 1 and 2 explain 64.5 % of the total variance within the polymicrobial mixtures. The different species combinations are spread out along the PCA plot. Additionally, the sample containing all the eight bacteria is not in close vicinity to the majority of the bacterial species. Rather, it is closer to the *Salmonella* species. These results confirm that our method is able to discriminate between individual bacterial species effectively.

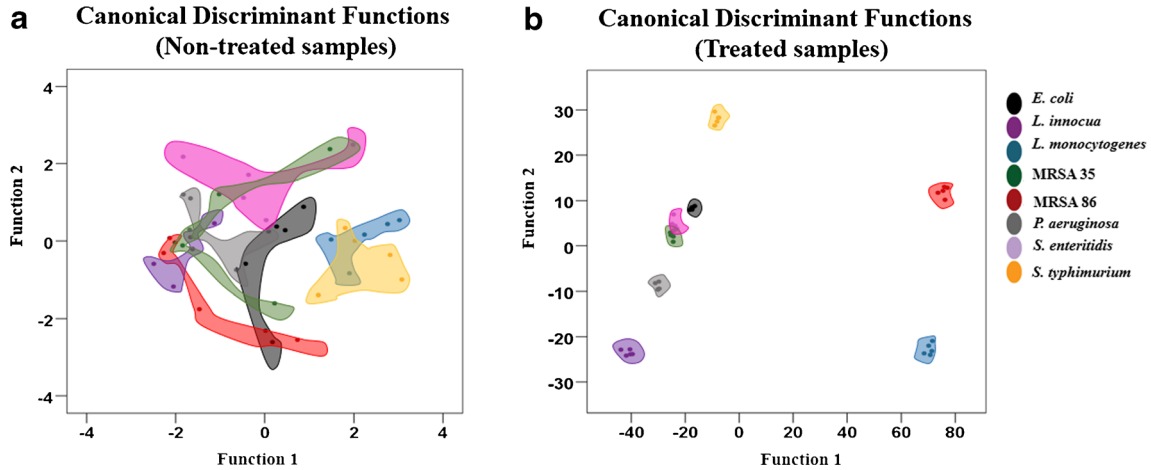

Fig. 5 Scatter plot derived from cross-validated linear discriminant analysis (LDA) analysis scores for the **a** non-treated and **b** the silver nanoparticle-Triton mixture treated bacterial culture samples. RAMAN spectra are reduced to single points with LDA and are plotted with 95 % confidence intervals

The next stage involved testing whether the method is able to detect Gram-negative versus Gram-positive bacteria. As observed, factors 1 and 2 explain 72.6 % of the total variance present in the polymicrobial mixtures. The PCA plots indicate the presence of clustering for *S. tymphirium*/*L. monocytogenes*, *L. innocua*/*E. coli*, *S. tymphirium*/*MRSA 86*, and *S. tymphirium*/*MRSA35*. The clustering effect may be caused by the data inputted into PCA or due to biological interactions within the polymicrobial culture.

In terms of the statistical analysis, PCA is only optimal when the variance within the samples is not extensive. For instance, factors 1 and 2 should be able to explain more than 72.6 % of the total variance present. Additionally, PCA is more effective when dealing with a small number of samples. There were 17 combinations of bacteria (Fig. 7b) which have been analyzed simultaneously using statistical methods. The developed assay can detect as low as 169 and 92 CFU per mL for MRSA 35 and *S. enteritidis* respectively, while up to 6 CFU per mL for *L. monocytogenes* and *L. innocua*, and about 2 CFU per mL for E. coli and *P. aeruginosa*. The limit of detection is 28 and 7 CFU per mL for MRSA 86 and *S. typhimurium* respectively.

On the other hand, describing and explaining the behavior of biological elements, such as bacterial interactions is extremely difficult. Researchers from various disciplines have theorized and tried to explain the mechanisms of action at work in polymicrobial cultures. For example, in cystic fibrosis models, iron acquiring *P.aeruginosa* outcompete *Salmonella* by depriving the latter of much needed iron. As a result, the growth of *Salmonella* growth is slowed while *Pseudomonas* is able to grow readily and perpetuate its own growth. When *Pseudomonas* "steals" iron from *Salmonella*, this triggers an increase in a molecule called *Pseudomonas* quinolone signal (PQS). This is but an example. Several other mechanisms may

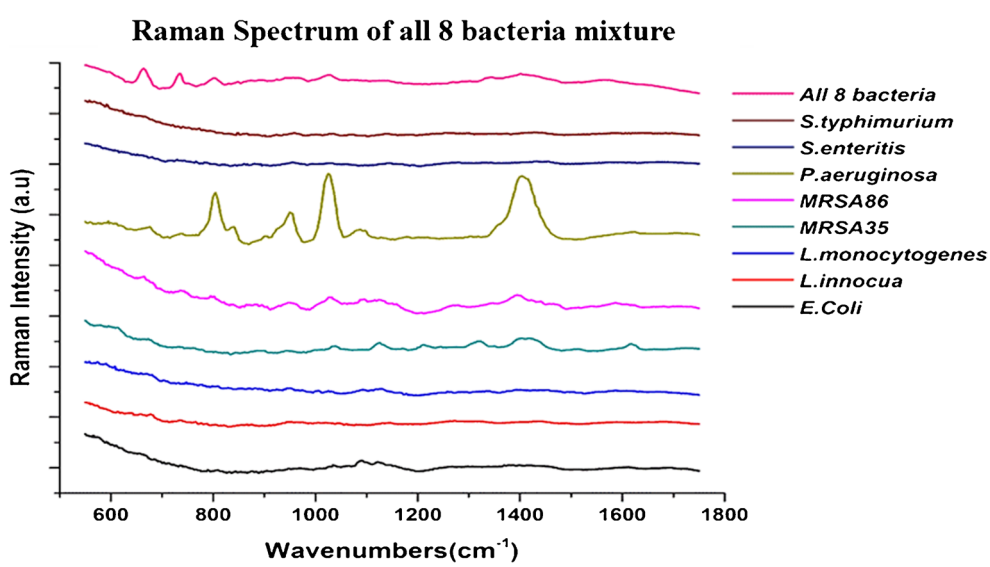

Fig. 6 Raman spectra of polymicrobial bacterial species and typical Raman spectra from individual bacterial colonies

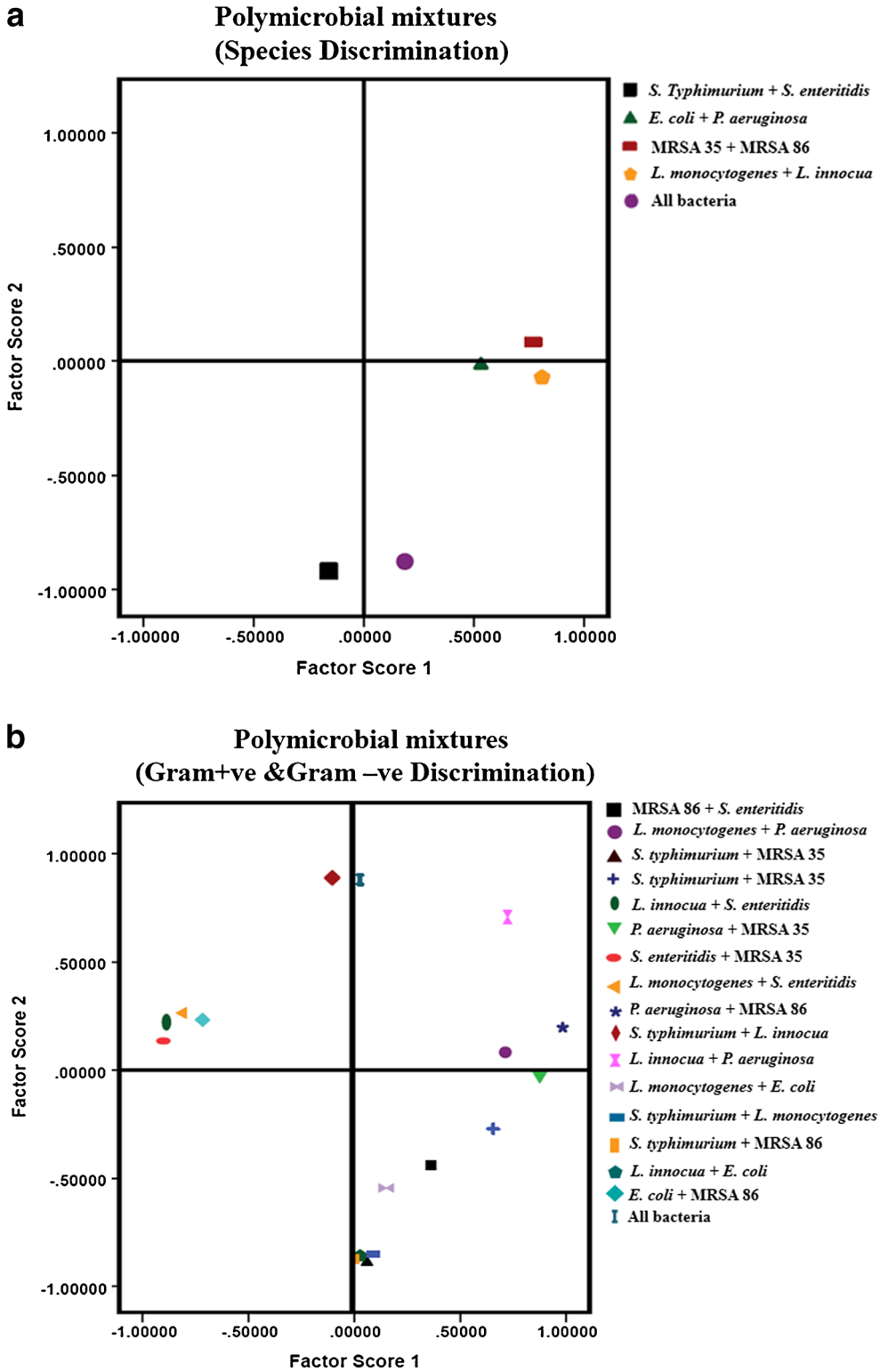

Fig. 7 **a** PCA output illustrating discrimination among polymicrobial bacterial pathogenic species. **b** PCA output illustrating Gram-negative and Gram-positive bacteria discrimination

explain the behavior of bacteria within a polymicrobial culture. These behaviors can be generally categorized as coexistence, dominance, or competition [24].

When analyzing the sample with all eight bacterial species (a complex community), it can be inferred that there are intra-species interactions that both promote competitive and cooperative strategies for species survival. Other possible cases may involve mutations, which can lead to variants that can adapt to certain niches. These niches are maintained by negative frequency-dependent selection. For instance, static

cultures of *P. fluorescens* generate several niche-specialized variants. One variant may overproduce extracellular polysaccharides (EPS), allowing the bacteria to float on the surface of the cultures to ultimately facilitate access of this variant to oxygen. However, this variant suffers if it becomes too dominant, as the mats can become too thick to float and then sink to the bottom of the culture [24]. As mentioned, the research into the mechanisms that foster bacterial interactions is limited, although there is growing interest in this field. Our goal was to design a set of protocols to detect and discriminate between bacterial species in a mixed culture for implementation in the food processing industry to readily and rapidly detect potentially harmful contaminants. To optimize these protocols and validate their effectiveness for industry use, it is imperative that we study intra-species bacterial interactions. Altogether this microfluidic based SERS biosensing assay integrating chemometric analysis provides improved analysis and species discrimination using Raman spectrometry.

Conclusions

We were able to effectively discriminate between eight different species of bacteria using a combination of chemometric analysis, microfluidic integrated SERS substrate, a bench top Raman instrument, and a set of protocols involving AgNP and Triton ×100. A series of peak assignments for each individual bacterial species was created and this forms the basis for unique fingerprinting of each species. Furthermore, the PCA output shows significant improvement in the identification of treated samples compared to the non-treated samples in monoculture solutions. The methods developed excel in separating eight relevant foodborne pathogen species under LDA analysis. Our protocols are successful in discriminating between species in complex polymicrobial solutions. However, there is still room for improvement for discriminating between Gram-negative and Gram-positive microorganisms. This study provides a desperately needed platform to detect and discriminate bacteria in the food industry that can be performed rapidly, on-site, and without huge overhead costs, unlike the currently available technologies.

Acknowledgments The authors sincerely thank the Natural Sciences and Engineering Research Council of Canada (4009929), Mitacs Globalink Program, and the Ontario Ministry of Research and Innovation (520512) for funding this study.

References

1. Griffiths M (2005) Understanding pathogen behaviour: virulence, stress response, and resistance. CRC Press, England
2. Centers for Disease Control and Prevention (2011) Estimates of Foodborne illness in the United States http://www.cdc.gov/Features/dsFoodborneEstimates/. Accessed 26 June 2015
3. Martins TD, Ribeiro ACC, Dias DL, Cavalcante HPM, de Camargo HS, da Costa Filho PA (2013) New insights on optical biosensors: techniques, construction and application. Intech, Croatia
4. Hendriksen RS, Vieira AR, Karlsmose S, Lo Fo Wong DM, Jensen AB, Wegener HC, Aarestrup FM (2011) Global monitoring of Salmonella serovar distribution from the World Health Organization global foodborne infections network country data bank: results of quality assured laboratories from 2001 to 2007. Foodborne Pathog Dis 8:887–900. doi:10.1089/fpd.2010.0787
5. Ibrahim SA, Asakir SF, Idris AA, Martinez-Urtaza J, Elsafi HH (2013) Prevalence of Salmonella species among asymptomatic food handlers in Khartoum State, Sudan. Br J Biomed Sci 70:88–89
6. Talabi AO, Etonyeaku AC, Sowande OA, Olowookere SA, Adejuyigbe O (2014) Predictors of mortality in children with typhoid ileal perforation in a Nigerian tertiary hospital. Pediatr Surg Int 30:1121–1127. doi:10.1007/s00383-014-3592-9
7. Noris M, Remuzzi G (2005) Hemolytic uremic syndrome. J Am Soc Nephrol 16:1035–1050. doi:10.1681/ASN.2004100861
8. Breidenstein EB, de la Fuente-Núñez C, Hancock RE (2011) Pseudomonas aeruginosa: all roads lead to resistance. Trends Microbiol 19:419–426. doi:10.1016/j.tim.2011.04.005
9. Centers for Disease Control and Prevention (2014) Pseudomonas aeruginosa in Healthcare Settings http://www.cdc.gov/hai/organisms/pseudomonas.html. Accessed 30 Aug 2015
10. Cartwright EJ, Jackson KA, Johnson SD, Graves LM, Silk BJ, Mahon BE (2013) Listeriosis outbreaks and associated food vehicles, United States, 1998–2008. Emerg Infect Dis 19:1–9. doi:10.3201/eid1901.120393
11. Wilder JR, Wegener DT, David MZ, Macal C, Daum R, Lauderdale DS (2014) A national survey of skin infections, care behaviors and MRSA nnowledge in the United States. PLoS One 19:e104277. doi:10.1371/journal.pone.0104277
12. Crago B, Ferrato C, Drews SJ, Svenson LW, Tyrrell G, Louie M (2012) Prevalence of Staphylococcus aureus and methicillin-resistant S. aureus (MRSA) in food samples associated with foodborne illness in Alberta, Canada from 2007 to 2010. Food Microbiol 32(1):202–205. doi:10.1016/j.fm.2012.04.012
13. Hoffmann S, Batz MB, Morris Jr JG (2012) Annual cost of illness and quality-adjusted life year losses in the United States due to 14 foodborne pathogens. J Food Protect 75:1292–1302. doi:10.4315/0362-028X
14. Schlosser E (2012) Fast food nation: the dark side of the all-American meal. Mariner Books, New York
15. Roda A, Mirasoli M, Roda B, Bonvicini F, Colliva C, Reschiglian P (2012) Recent developments in rapid multiplexed bioanalytical methods for foodborne pathogenic bacteria detection. Microchim Acta 178:7–28. doi:10.1007/s00604-012-0824-3
16. Kelley SO, Mirkin CA, Walt DR, Ismagilov RF, Toner M, Sargent EH (2014) Advancing the speed, sensitivity and accuracy of biomolecular detection using multi-length-scale engineering. Nat Nanotechnol 9:969–980. doi:10.1038/nnano.2014.261
17. Safavieh M, Ahmed MU, Tolba M, Zourob M (2012) Microfluidic electrochemical assay for rapid detection and quantification of Escherichia coli. Biosens Bioelectron 31:523–528. doi:10.1016/j.bios.2011.11.032
18. Innis MA, Gelfand DH, Sninsky JJ, White TJ (2012) PCR protocols: a guide to methods and applications. Academic Press, Waltham
19. Mühldorfer I, Schäfer KP (2001) Emerging bacterial pathogens (Vol. 8). Karger Medical and Scientific Publishers, Basel
20. Pieczonka NP, Aroca RF (2008) Single molecule analysis by surfaced-enhanced Raman scattering. Chem Soc Rev 37:946–954. doi:10.1039/B709739P

21. Chen L, Mungroo N, Daikuara L, Neethirajan S (2015) Label-free NIR-SERS discrimination and detection of foodborne bacteria by in situ synthesis of Ag colloids. J Nanobiotechnol 13:1–9. doi:10.1186/s12951-015-0106-4
22. Zhou H, Yang D, Mircescu NE, Ivleva NP, Schwarzmeier K, Wieser A, Haisch C (2015) Surface-enhanced Raman scattering detection of bacteria on microarrays at single cell levels using silver nanoparticles. Microchim Acta 182:2259–2266. doi:10.1007/s00604-015-1570-0
23. Juvé V, Cardinal MF, Lombardi A, Crut A, Maioli P, Pérez-Juste J, Vallée F (2013) Size-dependent surface Plasmon resonance broadening in nonspherical nanoparticles: single gold nanorods. Nano Lett 13:2234–2240. doi:10.1021/nl400777y
24. Hibbing ME, Fuqua C, Parsek MR, Peterson SB (2010) Bacterial competition: surviving and thriving in the microbial jungle. Nat Rev Microbiol 8:15–25. doi:10.1038/nrmicro2259
25. Sundaram J, Park B, Hinton A, Lawrence KC, Kwon Y (2013) Detection and differentiation of Salmonella serotypes using surface enhanced Raman scattering (SERS) technique. J Food Meas Charact 7:1–12. doi:10.1007/s11694-012-9133-0
26. Su L, Zhang P, Zheng D, Wang Y, Zhong R (2015) Rapid detection of *Escherichia coli* and *Salmonella typhimurium* by surface-enhanced Raman scattering. Optoelectron Lett 11:157–160. doi:10.1007/s11801-015-4216-x
27. Wang J, Xie X, Feng J, Chen JC, Du X, Luo J, Lu X, Wang S (2015) Rapid detection of Listeria monocytogenes in milk using confocal micro-Raman spectroscopy and chemometric analysis. Int J Food Microbiol 204:66–74. doi:10.1016/j.ijfoodmicro.2015.03.021